Adaptive strain-boost hyperdynamics simulations of stress-driven atomic processes

Shotaro Hara[1,2] and Ju Li[2,*]
[1]*Department of Mechanical Engineering, The University of Tokyo, Tokyo 113-8656, Japan*
[2]*Department of Materials Science and Engineering, University of Pennsylvania, Philadelphia, Pennsylvania 19104-6272, USA*
(Received 2 November 2010; published 19 November 2010)

The deformation and failure phenomena of materials are the results of stress-driven, thermally activated processes at the atomic scale. Molecular-dynamics (MD) simulations can only span a very limited time range which hinders one from gaining full view of the deformation physics. Inspired by the Eshelby transformation formalism, we present here a transformation "strain-boost" method for accelerating atomistic simulations, which is often more efficient and robust than the bond-boost hyperdynamics method [R. A. Miron and K. A. Fichthorn, J. Chem. Phys. **119**, 6210 (2003)] for exploring collective stress-driven processes such as dislocation nucleation, that have characteristic activation volumes larger than one atomic volume. By introducing an adaptive algorithm that safely maximizes the boost factor, we directly access the finite-temperature dynamical process of dislocation nucleation in compressed Cu nanopillar over time scale comparable to laboratory experiments. Our method provides stress- and temperature-dependent activation enthalpy, activation entropy and activation volume for surface-dislocation nucleation with no human guidance about crystallography or deformation physics. Remarkably, the accelerated MD results indicate that harmonic transition-state theory and the empirical Meyer-Neldel compensation rule give reasonable approximations of the dislocation nucleation rate.

DOI: 10.1103/PhysRevB.82.184114 PACS number(s): 61.72.Lk, 02.70.Ns, 46.15.−x, 62.20.M−

I. INTRODUCTION

The mechanical behavior of materials is well known to be temperature and strain-rate dependent.[1] This is fundamentally a reflection of the thermally activated nature of stress-driven processes, characterized by the stress σ and temperature T-dependent activation-free energy $Q(\sigma,T)$:[2] $R=\nu_{\mathrm{MEP}}\exp[-Q(\sigma,T)/k_{\mathrm{B}}T]$, where R is the success rate of a certain process, ν_{MEP} is the physical trial frequency along the minimum energy path (MEP), and k_{B} is the Boltzmann constant, assuming that transition-state theory (TST) (Ref. 3) holds. At laboratory strain rates typically in the range of $10^{-6}-10^{1}$ s^{-1}, the operative $Q(\sigma,T)$ is of the order $30k_{\mathrm{B}}T$. In contrast, the operative $Q(\sigma,T)$ explored in molecular dynamics (MD) simulations is of the order $5k_{\mathrm{B}}T-10k_{\mathrm{B}}T$, due to the considerably higher strain rates in the range of $10^{6}-10^{10}$ s^{-1}. Thus normal MD simulations may explore a completely different activation regime from the laboratory experiments, obscuring the interpretation of the simulation results.

Hyperdynamics[4] is an appealing scheme which potentially can accelerate atomistic simulations within the TST framework. As illustrated in Fig. 1, the acceleration can be attained by adding a positive boost potential $\Delta V(\mathbf{r})$ to the original interatomic potential $V(\mathbf{r})$ around its local minimum A, within one basin Γ_{A}, where $\mathbf{r}$ denotes the $3N$-dimensional configuration space for N-atoms system and Γ_{A} is the subset of all $\mathbf{r}$'s which "flows" to A by steepest descent upon release. Also, we define the $(3N-1)$-dimensional dividing surface bounding Γ_{A} as $\partial\Gamma_{\mathrm{A}}$, which consists of $(\Gamma_{\mathrm{A}}\cap\Gamma_{\mathrm{B}})$ segments for all neighboring local minima B's. For hyperdynamics to work, ΔV must be zero outside of Γ_{A}. As long as this requirement is satisfied, the MD trajectory with $V_{\mathrm{b}}=V+\Delta V$ is able to evolve with a time increment given by $\Delta t_{\mathrm{Phys}}=\Delta t_{\mathrm{MD}}e^{\Delta V/k_{\mathrm{B}}T}$, where Δt_{MD} is the time increment of the MD simulation (~fs) with $V_{\mathrm{b}}(\mathbf{r})$. The average speed-up factor is $\langle e^{\Delta V/k_{\mathrm{B}}T}\rangle_{\mathrm{b}}$, where $\langle\ \rangle_{\mathrm{b}}$ means averaging in the boosted-potential ensemble.

In the original hyperdynamics formulation, a Hessian-matrix-based boost potential is constructed, but it involves heavy computational overhead which limits its application so far to small-scale problems.[5] Miron and Fichthorn developed a simple geometry-based boost potential based on atomic nearest-neighbor bond lengths, called bond-boost hyperdynamics.[6] We have implemented this method, but found it to be unable of providing efficient boost for simulating dislocation nucleation, and also depends too sensitively on which atoms to boost. Here we propose a distinct strategy of designing the boost potential that allows us to safely simulate the finite-temperature deformation and failure in solids[7,8] with powerful speed-up, by incorporating the following ideas: (i) Eshelby inclusion and transformation picture,[9] (ii) least-square atomic-strain measure[10] (see also the Appendix), and (iii) adaptivity.

II. ADAPTIVE STRAIN-BOOST HYPERDYNAMICS

In geometry-based hyperdynamics such as the bond-boost[6] or strain-boost method, the boost potential $\Delta V(\mathbf{r})$ depends on local atomic geometry variables $\{s_i(\mathbf{r})\}$ assigned to atom i (or bond i), under the assumption that the dividing surface $\partial\Gamma_{\mathrm{A}}$ has distinct features in $\{s_i(\mathbf{r})\}$ that is easy to compute and identify. While changes in atomic pair distance, for instance, large irreversible change in bond length can be an indicator of basin hopping, they are not necessarily the most effective ones for identifying $\partial\Gamma_{\mathrm{A}}$. For example, change in bond angle cannot be reflected unless one considers a collection of three bond lengths together. Also, the boost potential $\Delta V(\mathbf{r})$ vanishes far away from the basin bottom and works the hardest when deviation from the equilibrium is still small, but in a self-equilibrating atomic

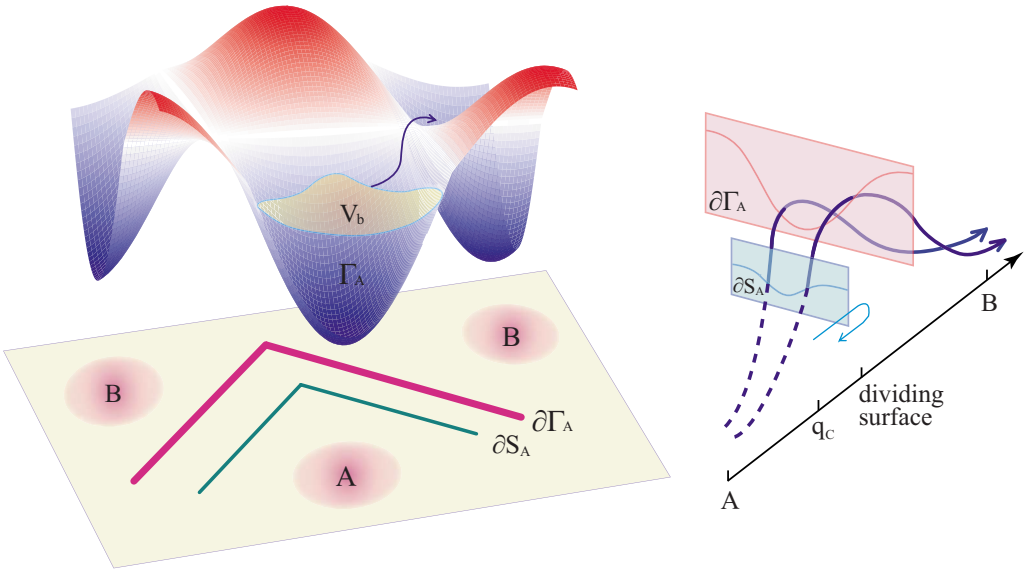

FIG. 1. (Color online) Illustration of the hyperdynamics scheme. Left figure shows a potential-energy surface (PES) and its two-dimensional projection map. To accelerate the transitions from minimum A to adjacent minimum B or B′ in hyperdynamics, one builds the new PES V_b by filling the basin Γ_A with the atomic-geometry-based boost potential. In hyperdynamics theorem, any modification of PES inside ∂S_A can be permitted as long as ∂S_A lies within Γ_A, where ∂S_A denotes the boundary surface on which the boost potential vanishes. Right figure illustrates an adaptive algorithm that allows us to optimize the position of ∂S_A by controlling the atomic-geometry-based threshold q_c. The maximum acceleration is achieved when ∂S_A is as close to the dividing surfaces $\partial \Gamma_A$ as possible near the relevant saddle points while not crossing the other saddle points.

lattice there is no energy-conjugate force to the bond length that is conceptually illuminating. The strain, in contrast, has been identified by Cauchy to be the energy conjugate variable of stress, which is obviously the primary driving force behind deformation and fracture. Hydrostatic strain is generally a good indicator of bond-length change, and the shear strains are good direct indicators of bond-angle change.

Thus, for *primarily stress-driven processes*, we accept the physical picture of the Eshelby transformation mechanics model,[9] in which the activation process is treated as an ellipsoidal inclusion of a certain size and shape that undergoes a transformation, as schematically illustrated in Figs. 2(a) and 2(b). For the transformation strain $\boldsymbol{\eta}_i$, we use the least-square measure of atomistic strain defined on each atom i (Ref. 10) (see also the Appendix), which minimizes among all possible local affine connections the error of mapping local atomic positions from reference to the current one, around atom i. In defining $\boldsymbol{\eta}_i$ one may use an arbitrary set of nearby atoms, regarded as the "Eshelby inclusion." The size of such strain-measuring (and subsequently strain-boosting) inclusions may be matched to the experimentally inferred spectrum of activation volume Ω,[11] and the shape may be targeted to the particular types of defects of interest. For instance, dislocation nucleation should correspond best to an oblate disk on certain crystallographic plane with high aspect ratio. However, to demonstrate the raw power of this method in exploring deformation physics, we purposefully omit all crystallographic and shape information in this paper, and just use a sphere with radius r_c in defining $\boldsymbol{\eta}_i$. Mathematical details about $\boldsymbol{\eta}_i$ and its first-order derivatives with respect to atomic positions can be found in the Appendix. It suffices to say here that $\boldsymbol{\eta}_i$ is a more collective (bond-angle aware) local geometric variable than the bond length, reflecting the condition of at least the nearest-neighbor atomic shell, with easily tunable additional collectivity.

Following Miron and Fichthorn,[6] the atomic-strain collective variables are then boosted by means of

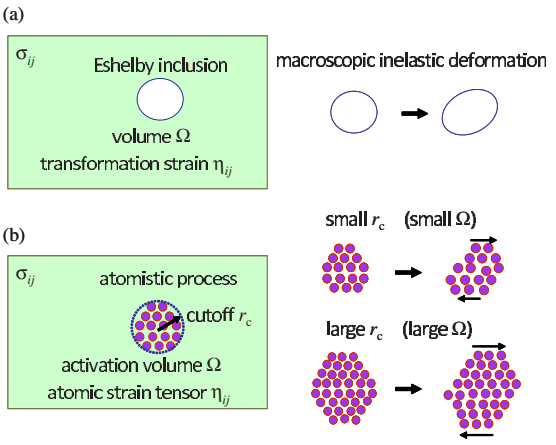

FIG. 2. (Color online) (a) Schematic of the classical Eshelby model. The ellipsoidal Eshelby inclusion with the size of Ω undergoes a transformation strain η_{ij} in the homogeneous stress field σ_{ij}. (b) Corresponding schematic of the transformation strain-boost method. The activation processes that involve more than one atom are treated like the Eshelby inclusion and the least-square measure of atomistic strain represents a transformation strain. The size of inclusions is chosen to match to the spectrum of activation volume Ω by flexibly changing the cutoff length r_c in defining the atomistic strain.

$$\Delta V(\mathbf{r}) = \frac{F(\eta_{\max}^{\mathrm{Mises}})}{N_{\mathrm{b}}} \sum_{i}^{N_{\mathrm{b}}} \delta V_i(\eta_i^{\mathrm{Mises}}). \quad (1)$$

Here, η_i^{Mises} is the von Mises shear tensor invariant of $\boldsymbol{\eta}_i$ (see the Appendix), δV_i is the boost potential in terms of $\eta_i^{\mathrm{Mises}}(\mathbf{r})$, N_{b} is the number of boost atoms and $F(\eta_{\max}^{\mathrm{Mises}})=1-(\eta_{\max}^{\mathrm{Mises}}/q_{\mathrm{c}})^2$ for $\eta_{\max}^{\mathrm{Mises}} \le q_{\mathrm{c}}$ and $F=0$ for $\eta_{\max}^{\mathrm{Mises}} > q_{\mathrm{c}}$, where $\eta_{\max}^{\mathrm{Mises}}=\max\{\eta_i^{\mathrm{Mises}}\}$ and q_{c} is the boost strain threshold.

$F(\eta_{\max}^{\mathrm{Mises}})$ is the shutdown function of the boost potential, therefore q_{c} prescribes the size of the boundary ∂S_{A} of the boosted region in Fig. 1. For the requirement $\Delta V=0$ on $\partial\Gamma_{\mathrm{A}}$, q_{c} must be small enough to guarantee that ∂S_{A} dose not touch $\partial\Gamma_{\mathrm{A}}$ (i.e., $\partial S_{\mathrm{A}} \subset \Gamma_{\mathrm{A}} \backslash \partial\Gamma_{\mathrm{A}}$), otherwise the hyperdynamics scheme breaks down. On the other hand, q_{c} should be large as possible to gain a maximum efficiency. Here, we give a simple adaptive algorithm that enables us to quickly search the optimal value of $q_{\mathrm{c}}=q_{\mathrm{c}}^{\max}$, which amounts to isotropic scaling the size of ∂S_{A} in Fig. 1 and checking which is the largest possible size that allows the most boosting ("efficiency") without having ∂S_{A} touch $\partial\Gamma_{\mathrm{A}}$ ("safety"). In this algorithm, MD simulations are carried out with V_{b} consisting of the boost potential ΔV with a variable q_{c}. By applying a strongly repulsive potential $\delta V_i=\alpha(q_{\mathrm{c}}-\eta_i^{\mathrm{Mises}})^2$, the system is driven to sample near ∂S_{A} and likely to escape from basin Γ_{A}. It is noted that while this repulsive potential becomes positive when $\eta_{\max}^{\mathrm{Mises}} > q_{\mathrm{c}}$, the boost potential ΔV is enforced to be zero due to the shutdown function. The stiffness α, which is independent of the $q_{\mathrm{c}}^{\max}$, can be set properly by monitoring the time variation in η_i^{Mises}. Then, $q_{\mathrm{c}}^{\max}$ is computed with the following recipe.

(i) Increase q_{c} from zero with an increment of Δq until the trajectory successfully finds a new basin Γ_{B}. The transition from Γ_{A} to Γ_{B} can be detected by monitoring the time evolution of $\eta_{\max}^{\mathrm{Mises}}$. Then, record the q_{c} value when the transition takes place and employ it as a first guess $q_{\mathrm{c}}^{\mathrm{trial}}$ for next step (ii).

(ii) Obtain five different trajectories going from Γ_{A} to Γ_{B} by performing the constant $q_{\mathrm{c}}=q_{\mathrm{c}}^{\mathrm{trial}}$ runs with random initial conditions. For each trajectory, check the hyperdynamics requirement of $\partial S_{\mathrm{A}} \subset \Gamma_{\mathrm{A}} \backslash \partial\Gamma_{\mathrm{A}}$. To judge this, quench the system at any time t when the trajectory $\mathbf{r}(t)$ passes through ∂S_{A} (i.e., when $\eta_{\max}^{\mathrm{Mises}}=q_{\mathrm{c}}^{\mathrm{trial}}$ is satisfied) and confirm whether the system always falls into the minimum A.

(iii) If (ii) holds for all five trajectories, we accept $q_{\mathrm{c}}^{\mathrm{trial}}$ as statistically valid $q_{\mathrm{c}}^{\max}$. Otherwise, update $q_{\mathrm{c}}^{\mathrm{trial}}$ by a small decrement of Δq and repeat step (ii) until the $q_{\mathrm{c}}^{\max}$ can be determined.

We have checked the statistics on how many trajectories should be taken into account in determining $q_{\mathrm{c}}^{\max}$. Compared with the $q_{\mathrm{c}}^{\max}$ value estimated from the five trajectories case, we found that the value from the three trajectories case is overestimated while the same value is obtained from the ten trajectories case. Thus, we judge that five trajectories are enough.

The adaptive algorithm above is treated as a preconditioning technique that makes the subsequent hyperdynamics simulations safe. At this stage, the boost potential has been changed to a function form of $\delta V_i=V_{\max}[1-(\eta_i^{\mathrm{Mises}}/q_{\mathrm{c}}^{\max})^2]$, where $V_{\max}$ is the magnitude of the total boost potential.[6]

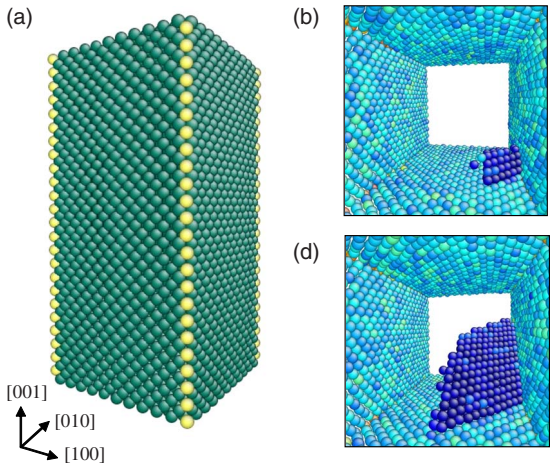

FIG. 3. (Color online) (a) Atomistic configuration of Cu nanopillar model used in adaptive strain-boost hyperdynamics simulations. The atoms within outermost layer (surface atoms) are not represented. The boost potential is assigned to the atoms along four corners (yellow). (b) Typical snapshot during the simulation under $T=180$ K and $\sigma=1.75$ GPa condition. Only the surface atoms and the atoms swept by dislocation are shown using central symmetry parameter. After repeating the appearance and disappearance of the Shockley partial dislocation embryo on the $\{111\}\langle 11\bar{2}\rangle$ slip systems from sharp corner, one embryo attains to its transition state at about $t_{\mathrm{Phys}}=70$ s, (c) followed by the rapid expansion of the dislocation loop.

III. SURFACE-MEDIATED DISLOCATION NUCLEATION MODEL

To illustrate the validity of the adaptive strain-boost method, we have studied the dislocation nucleation event in Cu nanopillar compression.[12] The atomistic configuration of the computational model is presented in Fig. 3(a). The system contains 13 824 Cu atoms and the cell sizes are $4.3\times4.3\times8.2$ nm^3. The crystallographic directions along the cell are the $x=[100]$, $y=[010]$, and $z=[001]$ directions. Periodic boundary condition is imposed along z direction and the others are traction-free surfaces. The Mishin potential[13] was employed to describe the Cu-Cu interaction. The compressive stress σ was imposed by applying the uniaxial constant strain along the [001] axis. The five different stress states in the range from 1.75 ($\approx 0.47\sigma_{\mathrm{ath}}$) to 2.50 ($\approx 0.67\sigma_{\mathrm{ath}}$) GPa are prepared, where $\sigma_{\mathrm{ath}}=3.75$ GPa is an athermal limit and corresponds to a critical value when a dislocation spontaneously nucleates without the aid of thermal fluctuation at 0 K.[2] This stress preferably induces the nucleation of the leading Shockley partial dislocation on the $\{111\}\langle 11\bar{2}\rangle$ slip systems, originated from the atomically sharp corner[12] [Figs. 3(b) and 3(c)].

To compute a local von Mises shear-strain invariant η_i^{Mises}, the cut-off length r_{c} of η_i^{Mises} was chosen as 4.8 Å. This involves about 30 neighbor atoms for each atom i, which is the same order of the activation volume Ω of the

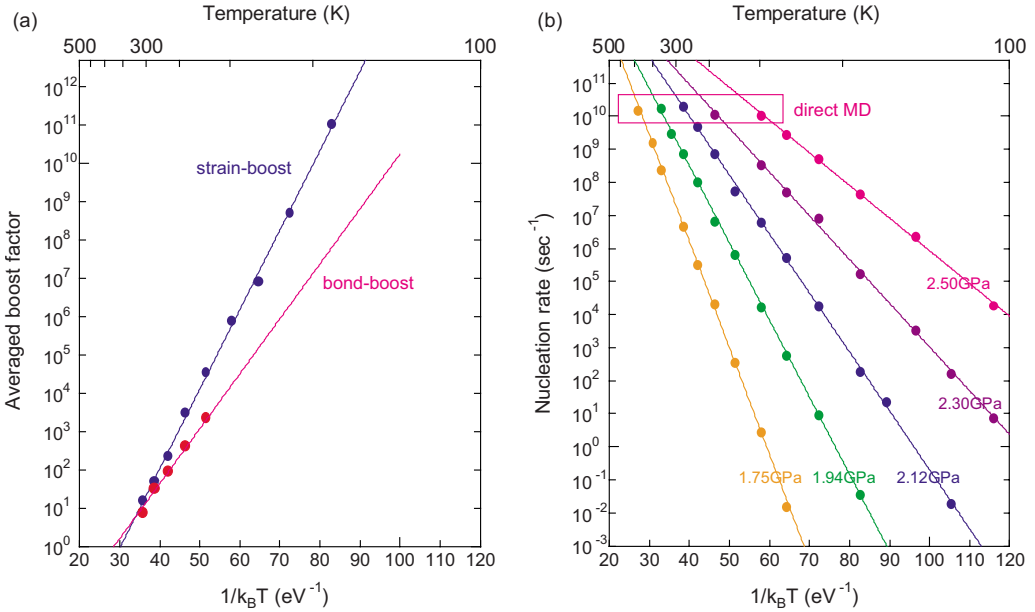

FIG. 4. (Color online) (a) Arrhenius plots of the averaged boost factor for dislocation nucleation from surface under compressive stress of 1.94 GPa. The data are measured by strain-boost method and bond-boost method, respectively. In these simulations, $q_c^{max}=0.095$ and 0.315 are employed, respectively. (b) Stress and temperature dependence of the dislocation nucleation rate $R(\sigma,T)$. Each R is calculated by $R=1/\tau_{ave}$, where τ_{ave} is the transition time averaged over 25 samples. Arrhenius fitting gives the measurement of activation enthalpy $Q_0(\sigma)$ of 0.74 eV, 0.54 eV, 0.41 eV, 0.31 eV, and 0.23 eV for 1.75 GPa, 1.94 GPa, 2.12 GPa, 2.30 GPa, 2.50 GPa, respectively. The apparent prefactor $R_0(\sigma)$ of 1.41×10^{19}, 6.87×10^{17}, 1.37×10^{17}, 1.81×10^{16}, and 6.62×10^{15} s^{-1} are also obtained in the same order.

dislocation nucleation, estimated from the recent mechanistic and computational modeling.[11,14] In this model, one may think it is natural to directly boost all the corner atoms at the outermost layer. However, because the least-square atomic strain η_i^{Mises} does not characterize coordination-deficient atoms well, the equivalent atoms to the corner atoms located at the second layer are boosted, as shown in Fig. 3(a).

For each stress state, the optimal q_c^{max} was determined using the adaptive algorithm with the parameters of $\Delta q=0.005$ and $\alpha=1000.0$ eV. Subsequently, we have constructed the boost potential with a function form of $\delta V_i=V_{max}[1-(\eta_i^{Mises}/q_c^{max})^2]$. Here, not only q_c but also V_{max} affects the achievable boost factor. Generally, larger V_{max} leads to larger boost factor. However, if V_{max} is too large, the statistical averaging $\langle e^{\Delta V/k_BT}\rangle_b$ becomes noisy.[6] To avoid this problem, V_{max} has been determined by performing short hyperdynamics runs (~50 ps) under the given temperature and stress conditions. For various V_{max}, we have checked the quality of ensemble average $\langle e^{\Delta V/k_BT}\rangle_b$ by computing the slope between the physical time t_{Phys} and simulation time t_{MD} (i.e., correlation coefficient λ). Practically, the adequate V_{max} value was defined under the criterion that λ of more than 80% of samples among all samples is larger than 0.95.

IV. RESULTS AND DISCUSSION

First, we show the computational speed-up achieved by the adaptive strain-boost hyperdynamics in terms of the averaged boost factor $\langle e^{\Delta V/k_BT}\rangle_b$. In Fig. 4(a), the boost factor under the typical stress $\sigma=1.94$ GPa is plotted over the temperature range where the nucleation event can be observed within one million simulation steps for all 25 samples. We find that as the temperature decreases, the boost factor exponentially increases up to 10^{11}. This dramatic acceleration indicates that the boost potential becomes strikingly effective for dislocation nucleation event and has an ability to track relevant dynamics extending over experimental time scale (seconds). We also presents the boost factor by the adaptive bond-boost hyperdynamics, in which the boost potential is assigned to all bonds connected with the atoms boosted in the strain-boost method. The comparison clearly shows that the strain-boost method is more efficient than the bond-boost method and the difference in the maximum achievable boost factor attains to about 8 orders of magnitude. This difference attests that the strain-boost method is more suitable for exploring the thermally activated collective motion of many atoms, such as dislocation nucleation. Note that in neither method did we give any crystallographic or deformation physics input as to what should happen, unlike the free-end nudged elastic band (FENEB) calculation[11] where mechanics intuition is necessary in designing the initial guess path.

Miron and Fichthorn examined the scaling of the boost factor with the number of boost bonds N_b. In the bond-boost method, they found that the boost-factor scale as $N_b^{-0.9}$ for the largest V_{max}.[6] Similarly, using the strain-boost method, we measured the boost-factor dependence on the number of boost atoms N_b by preparing the longer pillar systems in the z direction. As a result, we found that the boost factor approximately scales as $N_b^{-1.0}$, which is nearly identical to the bond-boost method. Thus, the advantages in the strain-boost method described above would not change even for the larger N_b system.

Next, we show the Arrhenius plot of the nucleation rate R at given stress ($\sigma=1.75-2.50$ GPa) and temperature

(T=100–450 K) in Fig. 4(b). We also give the nucleation rates directly computed by a normal MD (i.e., ΔV=0) for each stress, although the data are available only for the relatively high temperatures, reflected by the limited time scale (~ns). In contrast, owing to the large boost factor (~10^{11}), our hyperdynamics simulations provide the nucleation rate over considerably wider temperature range. Consequently, we have found the important result that the nucleation rate at each stress beautifully exhibits a pure Arrhenius behavior. This fact suggests that the harmonic approximation of TST [HTST (Ref. 15)] would be applicable to describe the dislocation nucleation process over the investigated temperature range. We also emphasize that the data points for the strain-boost method lie on the same straight line with those for a normal MD, demonstrating that our boosted model works completely accurately without blocking the equivalent paths for corner nucleation.

We now compare our numerical results with HTST and give the activation parameters associated with the surface-mediated dislocation nucleation. Within TST, the rate for a stress-driven thermally activated process can be expressed as[12]

$$R(\sigma,T) = M\nu_{\mathrm{MEP}}(\sigma)\exp\left(-\frac{Q(\sigma,T)}{k_{\mathrm{B}}T}\right), \tag{2}$$

where M is the number of the equivalent nucleation sites. HTST states that the temperature dependence of the activation-free energy $Q(\sigma,T)$ is simple and can be decomposed into,

$$Q(\sigma,T) = Q_0(\sigma) - TS(\sigma), \tag{3}$$

where $Q_0(\sigma)$ is the stress-dependent activation enthalpy that corresponds to the activation-free energy at T=0 K and $S(\sigma)$ is the stress-dependent activation entropy[15] related to the $3N-1$ vibrational frequencies the saddle point and A. Assuming Eq. (3) is true, one would have

$$R(\sigma,T) = R_0(\sigma)\exp\left(-\frac{Q_0(\sigma)}{k_{\mathrm{B}}T}\right) \text{ with}$$
$$R_0(\sigma) = M\nu_{\mathrm{MEP}}(\sigma)\exp\left(\frac{S(\sigma)}{k_{\mathrm{B}}}\right). \tag{4}$$

We emphasize that fitting to the hyperdynamics results in Fig. 4(b) provides us the more accurate evaluation of $Q_0(\sigma)$ and $R_0(\sigma)$ than fitting to the MD result only, due to the larger temperature range accessible. We give the result of $Q_0(\sigma)$ in Fig. 5(a) and compare with those computed from FENEB technique which is another probe for identifying the $Q_0(\sigma)$ and MEP via T=0 K calculation.[16,17] We confirm that our hyperdynamics $Q_0(\sigma)$ agree well with the FENEB $Q_0(\sigma)$ within 0.02 eV, validating HTST.

To our knowledge, calculation of the stress-dependent activation entropy $S(\sigma)$ has not been reported for dislocation nucleation or other problems. Here, we have obtained $S(\sigma)$ through Eq. (4) by taking $M=2N_{\mathrm{b}}$ and $\nu_{\mathrm{MEP}}(\sigma)=1.0\times10^{11}-3.0\times10^{11}$ s^{-1} that have been determined from the initial energy curvature along the MEP.[16] The result is provided in Fig. 5(b). We find that the activation

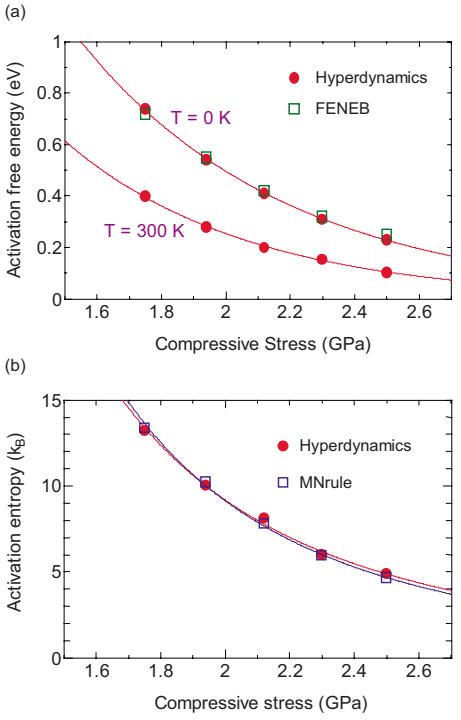

FIG. 5. (Color online) (a) Activation-free energy for dislocation nucleation from surface as a function of stress at T=0 and 300 K. For T=0 K case, the comparison with the FENEB results are shown. (b) Activation entropy as a function of stress. The prediction using empirical MN compensation rule is also presented. Best fit to our hyperdynamics results is obtained T_{MN}=625 K.

entropy increases as the stress decreases in the investigated stress range and is typically $4k_{\mathrm{B}}-14k_{\mathrm{B}}$. This means the saddle point is vibrationally more disordered than the basin minimum A, due to presumably more softer modes on the dividing surface $\partial\Gamma_{\mathrm{A}}$. Further, the estimation of $S(\sigma)$ allows us to evaluate the activation-free energy $Q(\sigma,T)$ at various temperatures. Importantly, our result indicates that, at room temperature, the entropic contribution to Eq. (3) is non-negligible and corresponds to about 40% of Q_0, as shown in Fig. 5(a). Likewise, the activation volume $\Omega(\sigma,T)=-\partial Q(\sigma,T)/\partial\sigma$, which characterizes the strain-rate sensitivity in materials plasticity,[11] has been derived. For instance, $\Omega=5b^3$ when Q=0.4 eV at room temperature, where b denotes the Burgers vector in Cu.

It is instructive to compare the computed $S(\sigma)$ with the Meyer-Neldel (MN) compensation rule,[18] which has been empirically discovered for many thermally activated processes in nature, including surface diffusion, electrical conduction, and grain boundary slip.[19,20] The comparison is motivated by the fact that its statistical validity has been a matter of debate and the discussions have been mostly based on experimental measurements.[20] According to MN, $S(\sigma)$ should be simply expressed as $S(\sigma)=Q_0(\sigma)/T_{\mathrm{MN}}$, where the T_{MN} is a characteristic temperature that is independent of the driving force (here stress). The physics behind MN was postulated to be due to multiple phonon combinatorics inside the activation volume.[21] In Ref. 12, the authors conjectured without substantial proof that T_{MN} should be close to the surface disordering temperature, since the local shear resis-

tance should decay to zero when the surface becomes disordered (premelted). The comparison is shown in Fig. 5(b). Surprisingly, the classic MN rule gives an excellent prediction of $S(\sigma)$ for this stress range with a best fitting parameter of $T_{\mathrm{MN}}=625$ K. We note that the MN rule is demonstrated in the form of stress dependence. The fitted T_{MN} corresponds to nearly half of the bulk melting point $T_{\mathrm{m}}(\sim 1350$ K),[22] which would be quite reasonable as the guess of surface disordering temperature, and is close to the value of 700 K taken in Ref. 12. Thus, our accelerated MD results strongly support the validity of (a) HTST and (b) MN rule for describing dislocation nucleation under a wide range of temperatures and stresses.

V. OUTLOOK

We have developed an atomic-strain-based, adaptive hyperdynamics method inspired by the Eshelby inclusion picture that is robust and efficient for exploring finite-temperature deformation and failure processes that critically involve more than one atom at the activated state. The flexibility in choosing the Eshelby inclusion size and shape for atomic-strain estimation and subsequent boosting is particularly advantageous when partial experimental information is available (activation volume spectrum inferred experimentally from strain-rate sensitivity measurements,[11] and known deformation physics, for example, shear by dislocations, not dilatory cracking). Effectively, our method can put an "activation volume filter" and "deformation physics filter" on microscopic processes to be probed by accelerated MD, to roughly match the experimentally known spectrum and screen out irrelevant mechanisms. Preliminary studies indicate our method is also highly effective for automatic exploration of shear transformations in metallic glasses.[7]

ACKNOWLEDGMENTS

This research was partially supported by the Ministry of Education, Science, Sports and Culture, Grant-in-Aid for Young Scientists (B), Grant No. 21760065, 2010. J.L. was supported by NSF under Grant No. CMMI-0728069, and No. DMR-1008104, MRSEC under Grant No. DMR-0520020, ONR under Grant No. N00014-05-1-0504, and AFOSR Grant No. FA9550-08-1-0325.

APPENDIX: LEAST-SQUARE ATOMIC STRAIN AND ARTIFICIAL FORCES

We would like to define 3×3 deformation gradient matrix $\mathbf{J}_i$ and its irrotational component, the Lagrangian strain matrix

$$\boldsymbol{\eta}_i \equiv (\mathbf{J}_i\mathbf{J}_i^{\mathrm{T}} - \mathbf{I})/2, \tag{A1}$$

for each atom i, where $\mathbf{I}$ is the identity matrix. Since strain is by definition a relative quantity, one would need two atomic configurations, the reference $\{\mathbf{x}_i^0\}$ and the current $\{\mathbf{x}_i\}$, to compute $\mathbf{J}_i$ and $\boldsymbol{\eta}_i$. See Fig. 2: let us define integer N_i to be the number of atomic neighbors of atom i in the reference configuration. These neighbors may be chosen by a simple distance cutoff; or if the deformation physics is known *a priori*, more sophisticated rules, such as only the atomic neighbors on specific top and bottom slip planes.

For each neighbor j of atom i, their current separation vector is

$$\mathbf{d}_{ji} \equiv \mathbf{x}_j - \mathbf{x}_i, \tag{A2}$$

in Cartesian space, and their old separation was

$$\mathbf{d}_{ji}^0 \equiv \mathbf{x}_j^0 - \mathbf{x}_i^0. \tag{A3}$$

Here we adopt a row-vector convention, e.g., $\mathbf{x}_i$, $\mathbf{d}_{ji}$, etc., are row vectors. Following Ref. 10, we seek a local affine transformation matrix $\mathbf{J}_i$ that best maps

$$\{\mathbf{d}_{ji}^0\} \rightarrow \{\mathbf{d}_{ji}\}, \quad \forall \quad j \in N_i \tag{A4}$$

in the least-square sense. That is, although $\{\mathbf{d}_{ji}^0\}\rightarrow\{\mathbf{d}_{ji}\}$ cannot be achieved exactly by affine transformation, we can still seek the best $\mathbf{J}_i$ that maps the two sets of positions, by minimizing the total error

$$\sum_{j\in N_i} |\mathbf{d}_{ji}^0\mathbf{J}_i - \mathbf{d}_{ji}|^2 = \mathrm{Tr}\sum_{j\in N_i} (\mathbf{J}_i^{\mathrm{T}}\mathbf{d}_{ji}^{0\mathrm{T}} - \mathbf{d}_{ji}^{\mathrm{T}})(\mathbf{d}_{ji}^0\mathbf{J}_i - \mathbf{d}_{ji}). \tag{A5}$$

Performing arbitrary matrix variation $\delta\mathbf{J}_i^{\mathrm{T}}$ in the above, we get

$$0 = \mathrm{Tr}\ \delta\mathbf{J}_i^{\mathrm{T}} \sum_{j\in N_i} \mathbf{d}_{ji}^{0\mathrm{T}}(\mathbf{d}_{ji}^0\mathbf{J}_i - \mathbf{d}_{ji}). \tag{A6}$$

For the above to be true for any asymmetric $\delta\mathbf{J}_i^{\mathrm{T}}$, there has to be

$$0 = \sum_{j\in N_i} \mathbf{d}_{ji}^{0\mathrm{T}}(\mathbf{d}_{ji}^0\mathbf{J}_i - \mathbf{d}_{ji}) \rightarrow \mathbf{J}_i = \mathbf{V}_i^{-1}\mathbf{W}_i, \tag{A7}$$

where

$$\mathbf{V}_i \equiv \sum_{j\in N_i} \mathbf{d}_{ji}^{0\mathrm{T}}\mathbf{d}_{ji}^0, \quad \mathbf{W}_i \equiv \sum_{j\in N_i} \mathbf{d}_{ji}^{0\mathrm{T}}\mathbf{d}_{ji}. \tag{A8}$$

With the optimized $\mathbf{J}_i$, we can then compute the 3×3 Lagrangian strain matrix $\boldsymbol{\eta}_i$ by Eq. (A1). The observation-frame independent hydrostatic strain invariant is then

$$\eta_i^{\mathrm{hydro}} \equiv \mathrm{Tr}(\boldsymbol{\eta}_i)/3, \tag{A9}$$

and the local shear invariant is

$$\eta_i^{\text{Mises}} \equiv \sqrt{\text{Tr}(\boldsymbol{\eta}_i - \eta_i^{\text{hydro}}\mathbf{I})^2/2} = \sqrt{\eta_{iyz}^2 + \eta_{ixz}^2 + \eta_{ixy}^2 + \frac{(\eta_{iyy} - \eta_{izz})^2 + (\eta_{ixx} - \eta_{izz})^2 + (\eta_{ixx} - \eta_{iyy})^2}{6}}. \tag{A10}$$

The above, Eqs. (A1)–(A10), have already been implemented in the free visualization software ATOMEYE,[23] using standard nearest-neighbor cutoff distances for N_i. It requires the specification of two atomic configurations, the reference and the current.

Note that N_i should be large enough such that the 3×3 matrix $\mathbf{V}_i$ in Eq. (A8) is nonsingular and can be inverted for Eq. (A7). In fully dense, three-dimensional solids, the nearest-neighbor atomic shell is usually sufficient, but special care may need to be taken for atoms near surfaces, which are coordination deficient. The rank deficiency of $\mathbf{V}_i$ may be checked before the inversion operation $\mathbf{V}_i^{-1}$ takes place, by computing the determinant of $\mathbf{V}_i$. If $\det|\mathbf{V}_i|=0$, then N_i will have to be enlarged.

In the strain-boost method one not only needs the value of $\boldsymbol{\eta}_i$ but also its derivatives with respect to $\mathbf{x}_i$ and $\{\mathbf{x}_j\}$, in order to compute the analytical forces due to δV_i. This is not difficult, since $\mathbf{V}_i$ and $\mathbf{V}_i^{-1}$ depend on $\{\mathbf{d}_{ji}^0\}$, not $\{\mathbf{d}_{ji}\}$. Therefore $\mathbf{J}_i$ in Eq. (A7) is a linear function in $\{\mathbf{x}_j\}$. So $\partial\mathbf{J}_i/\partial\mathbf{x}_j$ is independent of $\{\mathbf{x}_j\}$ and can be precomputed. $\frac{\partial\delta V_i(\eta_i^{\text{Mises}})}{\partial\mathbf{x}_j}$ can then be computed analytically by the chain rule. Furthermore, because $\eta_i^{\text{Mises}}(\{\mathbf{x}_j\})$ is translationally and rotationally invariant, it can be shown that the artificial forces due to the boost potential $\delta V_i(\eta_i^{\text{Mises}})$ satisfy momentum conservation

$$\frac{\partial\delta V_i(\eta_i^{\text{Mises}})}{\partial\mathbf{x}_i} + \sum_{j\in N_i}\frac{\partial\delta V_i(\eta_i^{\text{Mises}})}{\partial\mathbf{x}_j} = 0 \tag{A11}$$

as well as angular-momentum conservation

$$\sum_{j\in N_i}(\mathbf{x}_j - \mathbf{x}_i)\times\frac{\partial\delta V_i(\eta_i^{\text{Mises}})}{\partial\mathbf{x}_j} = 0. \tag{A12}$$

Lastly, after implementing $\{\boldsymbol{\eta}_i\}$ and analytical forces in a working code, here is a method to check the correctness of the coding.

(1) Randomly perturb a reference configuration $\{\mathbf{x}_i^0\}$ by a finite amount, to $\{\mathbf{x}_i\}$.

(2) Verify that the $\{\eta_i^{\text{Mises}}\}$ values are computed correctly, by comparing with the numerical output from ATOMEYE.[23] The $\delta V_i(\eta_i^{\text{Mises}})$ values can then be computed straightforwardly, where programming mistake is unlikely.

(3) Generate yet another $1\times 3N$ random displacement vector $\Delta\mathbf{r}\equiv\{\Delta\mathbf{x}_j\}$, the norm of which should be small: $|\Delta\mathbf{r}|=10^{-7}$ Å. Here N is the total number of atoms in the supercell. Compute the ratio between two small numbers: $A\equiv V(\{\mathbf{x}_j+\Delta\mathbf{x}_j/2\})-V(\{\mathbf{x}_j-\Delta\mathbf{x}_j/2\})$ and $B\equiv-\Sigma_{j=1,\ldots,N}\mathbf{F}_j\cdot\Delta\mathbf{x}_j$, where $\mathbf{F}_j$ is computed by the analytical force subroutine at $\{\mathbf{x}_j\}$. If the force subroutine is correctly coded, the ratio A/B should be numerically very close to $1:|A/B-1|<10^{-6}$, by the central difference error estimation.

*Author to whom correspondence should be addressed; liju@seas.upenn.edu

[1] U. F. Kocks, A. S. Argon, and M. F. Ashby, Prog. Mater. Sci. **19**, 1 (1975).
[2] J. Li, MRS Bull. **32**, 151 (2007).
[3] H. Eyring, J. Chem. Phys. **3**, 107 (1935).
[4] A. F. Voter, Phys. Rev. Lett. **78**, 3908 (1997).
[5] A. F. Voter, F. Montalenti, and T. C. Germann, Annu. Rev. Mater. Res. **32**, 321 (2002).
[6] R. A. Miron and K. A. Fichthorn, J. Chem. Phys. **119**, 6210 (2003).
[7] C. A. Schuh and A. C. Lund, Nature Mater. **2**, 449 (2003).
[8] J. R. Rice and G. E. Beltz, J. Mech. Phys. Solids **42**, 333 (1994).
[9] J. D. Eshelby, Proc. R. Soc. London, Ser. A **241**, 376 (1957).
[10] F. Shimizu, S. Ogata, and J. Li, Mater. Trans., JIM **48**, 2923 (2007).
[11] T. Zhu, J. Li, A. Samanta, H. G. Kim, and S. Suresh, Proc. Natl. Acad. Sci. U.S.A. **104**, 3031 (2007).
[12] T. Zhu, J. Li, A. Samanta, A. Leach, and K. Gall, Phys. Rev. Lett. **100**, 025502 (2008).
[13] Y. Mishin, M. J. Mehl, D. A. Papaconstantopoulos, A. F. Voter, and J. D. Kress, Phys. Rev. B **63**, 224106 (2001).
[14] R. J. Asaro and S. Suresh, Acta Mater. **53**, 3369 (2005).
[15] G. H. Vineyard, J. Phys. Chem. Solids **3**, 121 (1957).
[16] G. Henkelman and H. Jonsson, J. Chem. Phys. **113**, 9978 (2000).
[17] S. Hara, S. Izumi, and S. Sakai, J. Appl. Phys. **106**, 093507 (2009).
[18] W. Meyer and H. Neldel, Z. Tech. Phys. (Leipzig) **12**, 588 (1937).
[19] N. F. Mott, Proc. Phys. Soc. London **60**, 391 (1948).
[20] A. Yelon, B. Movaghar, and R. S. Crandall, Rep. Prog. Phys. **69**, 1145 (2006).
[21] A. Yelon and B. Movaghar, Phys. Rev. Lett. **65**, 618 (1990).
[22] T. Frolov and Y. Mishin, Phys. Rev. B **79**, 045430 (2009).
[23] J. Li, Modell. Simul. Mater. Sci. Eng. **11**, 173 (2003).